NEUROPATHOLOGY

Neuropathology 2020; **40**, 546–558 doi:10.1111/neup.12

Original Article

Glioblastoma multiforme: Metabolic differences to peritumoral tissue and *IDH*-mutated gliomas revealed by mass spectrometry imaging

Judith M. Kampa,[1] Udo Kellner,[2] Christian Marsching,[3] Carina Ramallo Guevara,[3] Ulrich J. Knappe,[4] Mikail Sahin,[1] Marco Giampà,[1]* Karsten Niehaus[1] and Hanna Bednarz[1]

[1]Proteome and Metabolome Research, Faculty of Biology & Center for Biotechnology, Bielefeld University, Bielefeld, [2]Institut für Pathologie, Johannes Wesling Klinikum, [4]Klinik für Neurochirurgie, Johannes Wesling Klinikum, Minden and [3]Center for Mass Spectrometry and Optical Spectroscopy (CeMOS), Mannheim University of Applied Sciences, Mannheim, Germany

Glioblastoma multiforme (GBM) is the most common malignant primary brain tumor. High infiltration rates and poor therapy responses make it the deadliest glioma. The tumor metabolism is known to differ from normal one and is influenced through various factors which can lead to longer survival. Metabolites are small molecules (< 1500 Da) that display the metabolic pathways in the tissue. To determine the metabolic alterations between tumor and peritumoral tissue in human GBMs, mass spectrometry imaging (MSI) was performed on thin sections from 25 resected tumors. In addition, the GBMs were compared with six gliomas harboring a mutation in the isocitrate dehydrogenase (IDH1) gene (*IDH1*). With this technique, a manifold of analytes can be easily visualized on a single tissue section. Metabolites were annotated based on their accurate mass using high resolution MSI. Differences in their mean intensities in the tumor and peritumoral areas were statistically evaluated and abundances were visualized on the tissue. Enhanced levels of the antioxidants ascorbic acid, taurine, and glutathione in tumor areas suggest protective effects on the tumor. Increased levels of purine and pyrimidine metabolism compounds in GBM areas indicate the high energy demand. In accordance with these results, enhanced abundances of lactate and glutamine were detected. Moreover, decreased abundance of *N*-acetylaspartate, a marker for neuronal health, was measured in tumor areas. Obtained metabolic information could potentially support and personalize therapeutic approaches, hence emphasizing the suitability of MSI for GBM research.

Key words: antioxidants, glioblastoma multiforme, MALDI mass spectrometry imaging, spatial localization of metabolites, tumor metabolism.

INTRODUCTION

Glioblastoma multiforme (GBM) is the most common malignant primary brain tumor.[1] They are the most malignant form (WHO Grade IV) of astrocytomas, which is one of the main types of gliomas.[2] Current therapies include surgery, chemotherapy, and radiotherapy.[3,4] Nevertheless, GBM is the deadliest brain tumor, with a five-year survival rate of only 5.6%.[1] A reason for the high mortality rate of the disease is the infiltration in the surrounding parenchyma of the central nervous system (CNS), preventing complete resections. In addition, treatment is weakened through resistance of the tumor to radiation and chemotherapy.[5,6]

Improved therapeutic efficacy and a longer survival rate are associated with mutations in the isocitrate dehydrogenase 1/2 (IDH1/2) gene *(IDH1/2)* as well as with a methylation of the O-6-methylguanine-DNA methyltransferase (MGMT).[7,8] Other common molecular GBM markers like p53, phosphatase and tensin homolog (PTEN), phosphoinositide 3-kinase (PI3K), epidermal growth factor receptor (EGFR), and 1p/19q have an ambiguous prognostic importance.[7] While major metabolic changes in tumors include enhanced aerobic glycolysis, so-called the Warburg effect, and glutamine metabolism,[9,10] genomic and epigenetic

Correspondence: Hanna Bednarz, Proteome and Metabolome Research Bielefeld University Universitaetsstrasse 25, 33615 Bielefeld, Germany.
Email: hanna@cebitec.uni-bielefeld.de

*Present address: Norwegian University of Science and Technology Trondheim, Norway

Received 04 December 2019; revised 20 March 2020; accepted 22 March 2020; published online 13 July 2020.

alterations also modulate the metabolism in GBM.[11,12] The analysis of the GBM metabolism is gaining interest to improve diagnostic accuracy and to promote therapeutic effects.[13,14]

Molecular spectroscopy and mass spectrometry (MS) are common tools for the investigation of metabolites and metabolic alterations.[15] While most techniques require homogenized samples and do not provide information on spatial distributions of analytes in tissues, MS imaging (MSI) can be performed on thin sections. A frequently used MSI variant is matrix-assisted laser desorption/ionization (MALDI) MSI. Depending on the matrix, a manifold of analytes, such as small molecules, lipids and peptides, can be detected. Mass spectra are generated for every pixel by rasterization of the tissue. Recent studies using MALDI MSI in transmission mode have demonstrated lateral resolutions below one micrometer,[16] making single cell analysis possible.

In tumor research, MALDI MSI was already used for classification of protein expression status of human EGFR 2 (HER2) in breast cancer,[17] identification of prostate carcinoma,[18] and biomarker investigation in ovarian carcinomas.[19] In GBM research, MALDI MSI studies on metabolites were conducted in mouse models[20] and xenografts,[21] whereas metabolic analysis on human tissue seems to be unexplored.

In this study, 25 human GBM samples were analyzed using an MALDI MSI to elucidate and visualize differences in the metabolism compared to peritumoral tissue and to *IDH*-mutated gliomas. This emerging technique can reveal tumor biology and can hint towards new supporting mechanisms for therapeutic approaches while only a minimal amount of tissues are needed.

MATERIALS AND METHODS

Human material

Human GBMs were resected between 2017 and 2018 at the Johannes Wesling Klinikum Minden in Minden, Germany. The study was approved by the local ethics committee, registered with the *Bundesinstitut für Arzneimittel und Medizinprodukte*. Patients gave informed consent for the use of resected samples for scientific purposes. Patient samples were anonymized. A total of 31 tissue samples was snap-frozen and stored in liquid nitrogen until further use. The 25 GBMs (WHO Grade IV) were classified as *IDH* wild-type. The analyzed six lower graded gliomas (WHO Grades I-III) were confirmed with a mutation in *IDH1*. A detailed list of analyzed tumors can be found in the supplementary information (Table S1 and Table S2 in Appendix S1).

Sample preparation

Frozen tissues were sectioned at a thickness of 10 μm using a cryostat. Sections were placed onto conductive indium tin oxide (ITO) slides (Bruker Daltonik GmbH, Bremen, Germany), and consecutive sections were placed on regular microscope slides for histological staining. Cryo-sections for mass spectrometry imaging were dried in a desiccator and stored in a dry cabinet (Eureka Dry Tech/Taiwan Dry Tech, Taipei, Taiwan) until further use.

Histological staining

Hematoxylin and eosin (HE) staining was performed using a standard protocol. Stained sections were scanned using a MIRAX DESK scanner (Carl Zeiss Microscopy GmbH, Jena, Germany) and annotated by an experienced pathologist.

Matrix application

Dried tissue sections on ITO slides were coated with the matrix 1,5-diaminonaphthalene (DAN) hydrochloride (HCl). Matrix was prepared as described by Liu *et al.*, 2014.[22] The deposition of the matrix was performed using a TM-Sprayer (HTX-Technologies, LLC, Chapel Hill, NC, USA) at 14 passes with a velocity of 1200 mm/min and a flow rate of 0.1 mL/min at a nozzle temperature of 70°C. Further spraying parameters were 3-mm track spacing, crisscross pattern, and 0 s drying time.

MSI

Matrix-assisted laser desorption/ionization time-of-flight mass spectrometry imaging (MALDI-TOF-MSI) was performed on all 31 samples at a lateral resolution of 50 μm using a RapifleX (Bruker Daltonik GmbH) mass spectrometer for analyte distribution analysis. Measurements were executed over a mass range of m/z 50–1000, with 250 laser shots per pixel with the Smart Beam Laser under M5 small mode and with a sample rate of 1.25. Detector Gain was set to 2450 V and the pulsed ion extraction to 90 ns. Source as well as analyzer voltages were set as follows: ion source, 20 kV; PIE, 2.470 kV; lens, 11.100 kV; Ref 1, 20.950 kV; Ref 2, 1.085 kV; Ref 3, 8.550 kV. Mass calibration was performed using red phosphorus clusters.

High mass resolution imaging was performed with a solariX (Bruker Daltonik GmbH) FT-ICR-MS on one of the GBM samples with tumor and peritumoral regions at a 10-μm lateral resolution for the chemical identification of the analytes over a mass range of m/z 85–500. Spectra were recorded with a size of 8 M, which resulted in a mass resolution of 450 000 at m/z 400. For each pixel, four average scans each with 200 laser shots where used. Q1 mass was set to m/z 100, while time of flight was adjusted to 0.5 ms. External mass calibration was performed using red

phosphorus clusters. For internal lock mass calibration, the $[M\text{-}H]^-$ signal of DAN at m/z 157.077122 was used.

All measurements, using MALDI-TOF-MSI as well as matrix-assisted laser desorption/ionization Fourier transform ion cyclotron resonance mass spectrometry (MALDI-FT-ICR-MSI), were carried out in negative ion mode.

Data analysis

MSI data analysis was executed using an SCiLS Lab 2019c Pro software (Bruker Daltonik GmbH). For visualization of analytes, MALDI-TOF-MSI data was normalized to the total ion count (TIC). Regions of interest were selected according to pathological annotations on adjacent HE staining images and not normalized mean intensities were extracted.

Putative identification of the detected compounds was performed on high mass resolution imaging data in flexImaging 4.1 (Bruker Daltonik GmbH, Bremen, Germany) with an error of ≤ 1 ppm using the databases Metlin and Human Metabolome Database (HMDB). Identifications are listed in Table S3 in Appendix S1.

Statistical analysis

Statistical analysis was implemented in python 3.7.5 (Python Software Foundation). Mean intensities of GBMs ($n = 25$) and peritumoral ($n = 13$) regions, as well as *IDH*-mutated gliomas ($n = 6$), were visualized in boxplots with a lower whisker at 5% and an upper whisker at 95%. Statistical significance was calculated using an unpaired Student's *t*-test, and considered when a *P*-value was less than 0.05. As indicated in Figures 2–6, significant changes are labeled with an asterisk (*), while *P*-values > 0.05 are marked as not significant (ns).

RESULTS

GBM is characterized by diffuse infiltrative growth; hence, it is difficult to define clear border. HE staining of resected tissues revealed tumor-peritumoral tissue border in 13 of 25 samples. All 25 tissue samples contained dense tumor areas. Based on pathological annotations on HE staining images, regions of interest for peritumoral and tumor tissues were selected on subsequent sections for statistical analysis of MSI data. Necrotic tissues and inconclusive transitions between different areas were disregarded. Figure 1 shows the tissue selection for three representative examples of tissue sections from the resected GBMs.

Using the calculated mean intensities of the GBMs and peritumoral regions for statistical analysis revealed changes in antioxidants, fatty acids, purine and pyrimidine metabolism components, and important tumor or brain metabolites

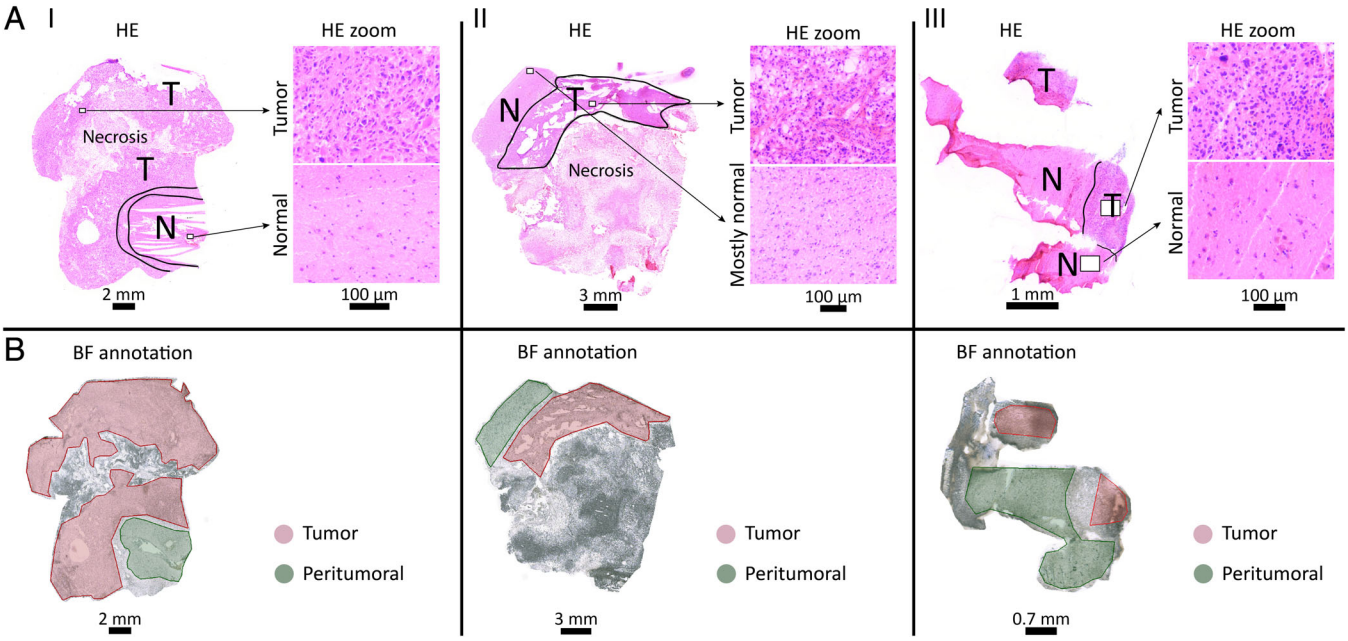

Fig 1 Histopathological analysis of HE-stained cryo-sections of three representative human GBMs (I-III). (A) On HE staining images and zooms in tumor, peritumoral normal tissues, whole tissue scans show annotations by a pathologist. (B) On brightfield (BF) image of adjacent tissue sections, measured by MSI, regions of tumor (red) and peritumoral tissue (green) are selected for quantitative metabolic analysis according to pathological annotations; necrotic and transition areas are disregarded.

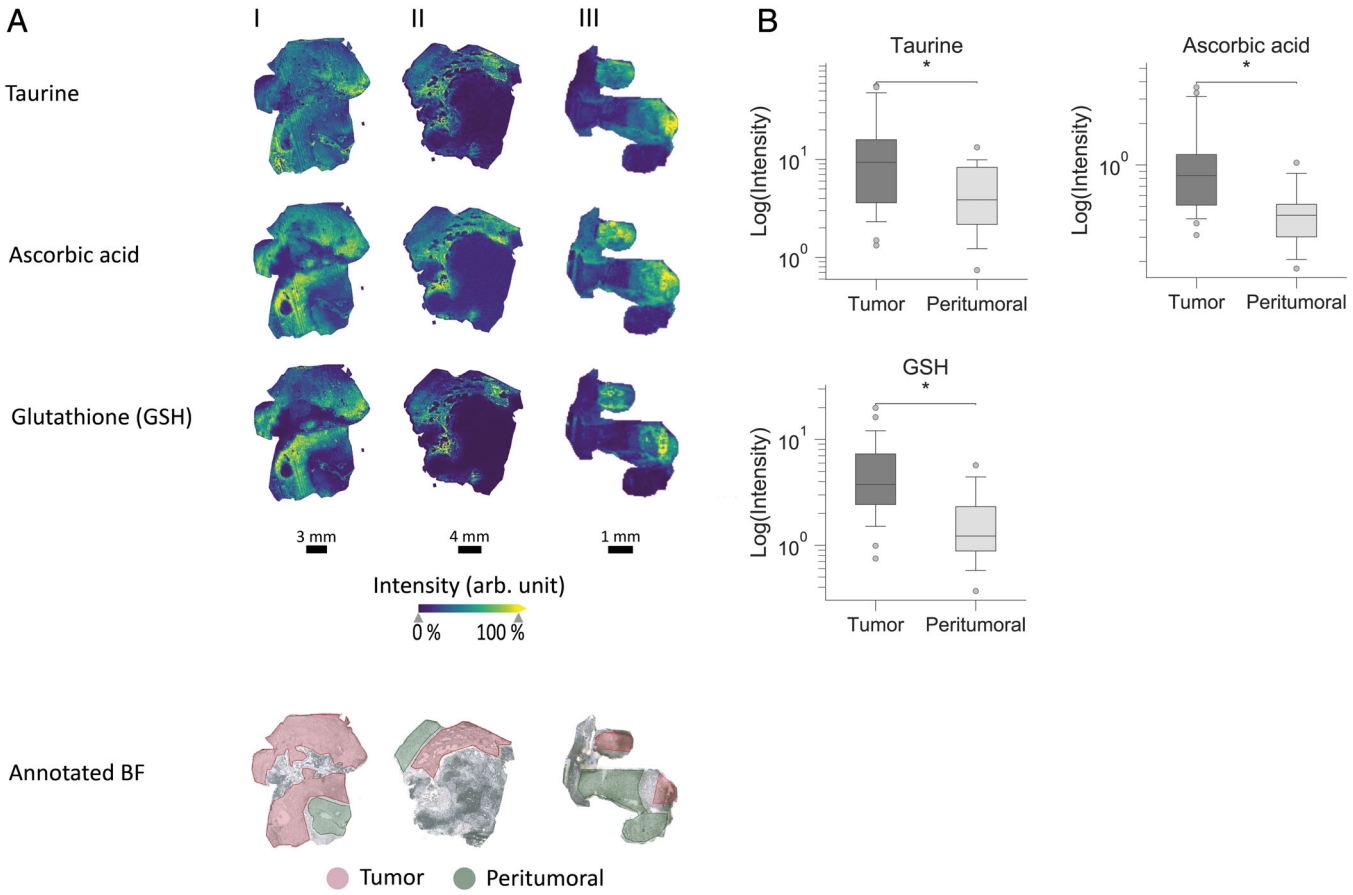

Fig 2 Analyses of antioxidants in tumor and peritumoral tissue areas of three examples (I-III) by MALDI-TOF-MSI (A) and intensity boxplots including all 25 GBM samples (B). (A) MALDI-TOF-MSI visualizes taurine, ascorbic acid, and GSH levels in three example tissue sections. An annotated brightfield (BF) is included for orientation on tissues. (B) Intensity boxplots for antioxidants shown in (A) demonstrate enhanced abundances of antioxidants. Asterisks indicate $P < 0.05$. Tumor group ($n = 25$), Peritumoral group ($n = 13$).

(Figs 2–5). Furthermore, comparison with *IDH*-mutated gliomas showed increased 2-hydroxyglutarate (2-HG) levels (Fig. 6).

Antioxidants are enhanced in GBM

The antioxidants taurine, ascorbic acid, and glutathione (GSH) were detected by MSI, which revealed the distribution within the tissues (Fig. 2). All three metabolites were annotated by their exact mass using MALDI-FT-ICR-MS (Table S3 in Appendix S1). Taurine tended to be significantly increased in the tumor areas, ($P = 0.049$). Ascorbic acid not only showed enhanced abundances in the tumor areas in the three given MSI examples but also appeared significantly altered when comparing all the 25 tumor areas with the 13 peritumoral areas ($P = 0.016$). Both taurine and ascorbic acid seemed to show a gradual transition from GBM to peritumoral areas. A similar significant increase ($P = 0.01$) was detected for GSH. The abundance appeared strongest in the center of the tumors.

Fatty acids show decreased intensities in tumor areas

Different fatty acids were found to be decreased in GBM areas compared to peritumoral tissue areas (Fig. 3). The detected ω-6 fatty acids arachidonic acid and adrenic acid were significantly decreased in the tumor tissue areas with *P*-values of 0.035 and 0.027, respectively. Both analytes were uniformly distributed in peritumoral tissue areas associated with almost absent intensities in tumor areas, although the value was weak in sample II. Further, ω-6 fatty acids linoleic acid (LA) and dihomo-γ-linolenic acid (DGLA) were not significantly changed in GBM areas. Ionic maps of stearic acid and oleic acids showed related distributions, although stearic acid showed a gradual transition from peritumoral to tumor areas. This leads to a

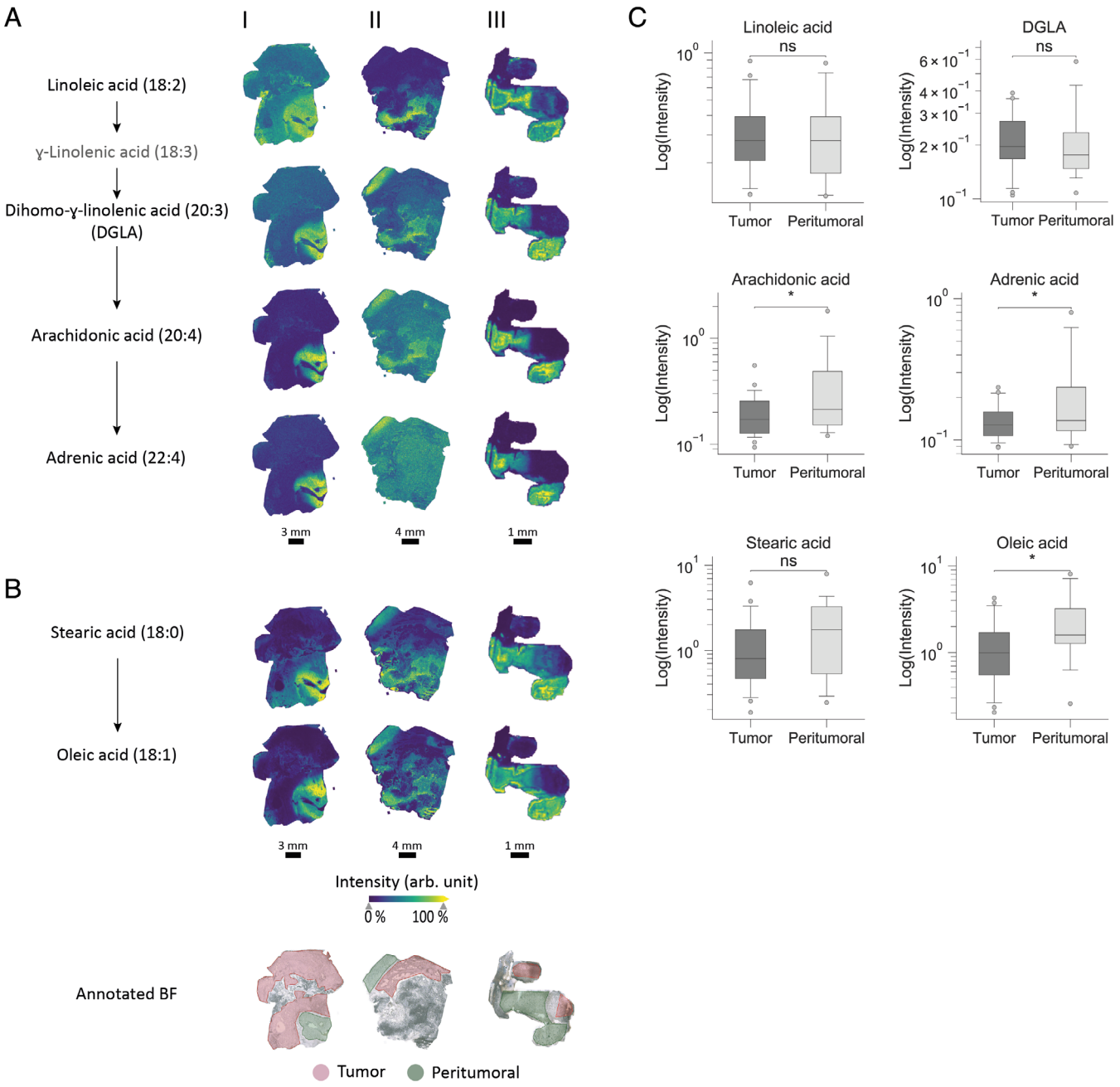

Fig 3 Analyses of fatty acids in tumor and peritumoral tissue areas of three examples (I–III) by MALDI MSI (A, B) and intensity boxplots including all 25 GBM samples (C). (A, B) MALDI-TOF-MSI visualizes ω-6 fatty acids linoleic acid (LA), dihomo-γ-linolenic acid (DGLA), arachidonic acid, and adrenic acid (A) and ω-9 fatty acids stearic acid and oleic acid (B). An annotated brightfield (BF) is included for orientation on tissues. (C) Intensity boxplots for fatty acids shown in (A) and (B) demonstrate a tendency of decreased levels of fatty acids. Measurements are performed in negative reflector mode with matrix DAN HCl. Asterisks indicate $P < 0.05$. ns, not significant. Tumor group ($n = 25$), Peritumoral group ($n = 13$).

calculated significant change in oleic acid intensities ($P = 0.034$) and no significant alteration for stearic acid.

Alterations in compounds of purine and pyrimidine metabolism

Metabolites of purine and pyrimidine metabolism were detected by MSI. The values of purine metabolism compounds, including ADP, AMP, and inosine, are shown in Figure 4A. The values of pyrimidine metabolism components, including UDP, UMP, and uridine, are shown in Figure 4B. Interestingly, ADP and UDP were both significantly increased in tumor areas with *P*-values of 0.032 and 0.017, respectively, and were mostly located distantly to peritumoral tissue areas. AMP and UMP also showed significantly

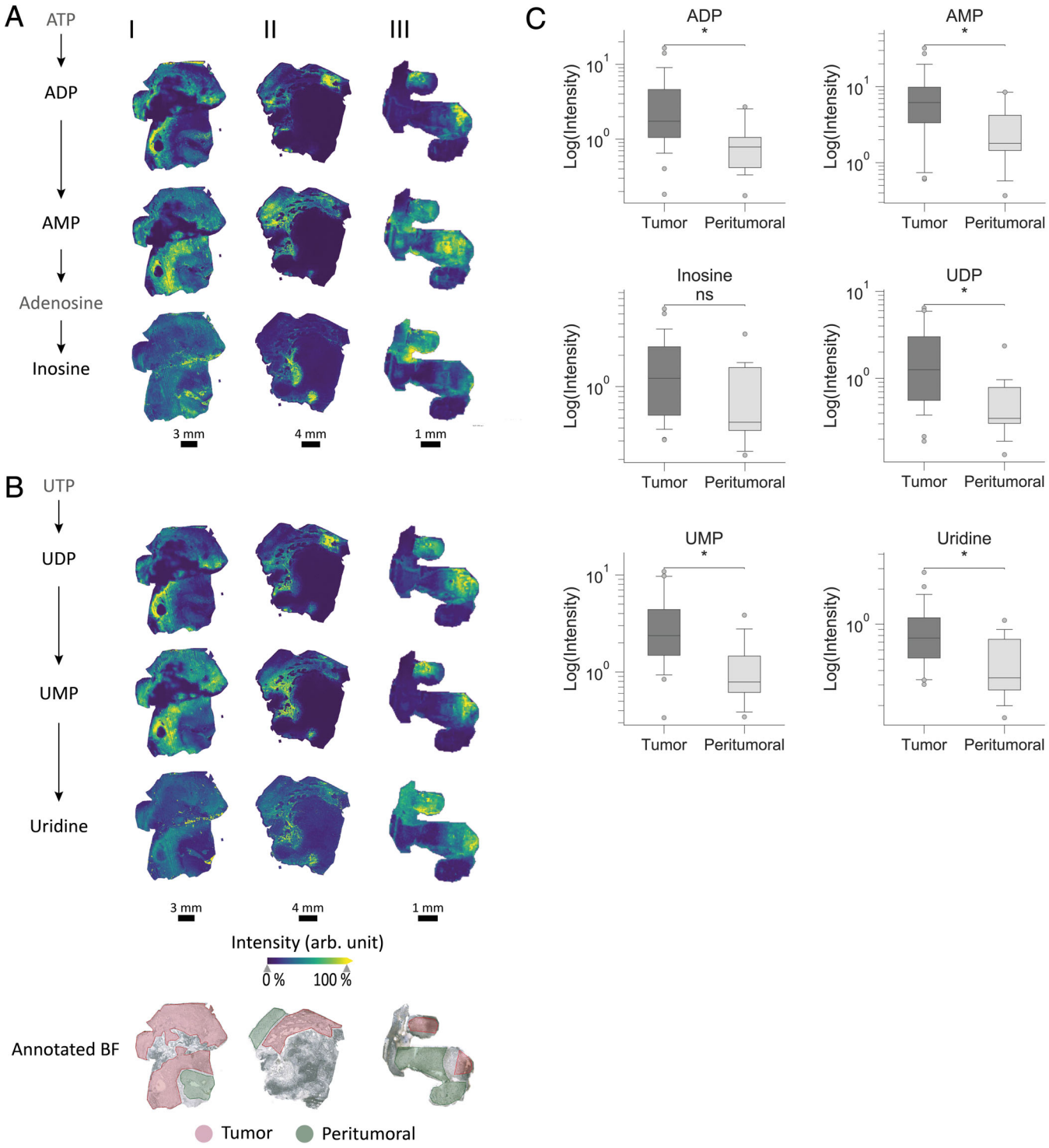

Fig 4 Analyses of purine (A) and pyrimidine (B) metabolites in tumor and peritumoral tissue areas of three examples (I–III) by MALDI MSI (A, B) and intensity boxplots including all 25 GBM samples (C). (A, B) MALDI-TOF-MSI visualizes ADP, AMP, and inosine (A) as well as UDP, UMP, and uridine (B). An annotated brightfield (BF) is included for orientation on tissues. (C) Intensity boxplots for the metabolites shown in (A) and (B) demonstrate a tendency of increased levels. Measurements are performed in negative reflector mode with matrix DAN HCl. Asterisks indicate $P < 0.05$. ns, not significant. Tumor group ($n = 25$), Peritumoral group ($n = 13$).

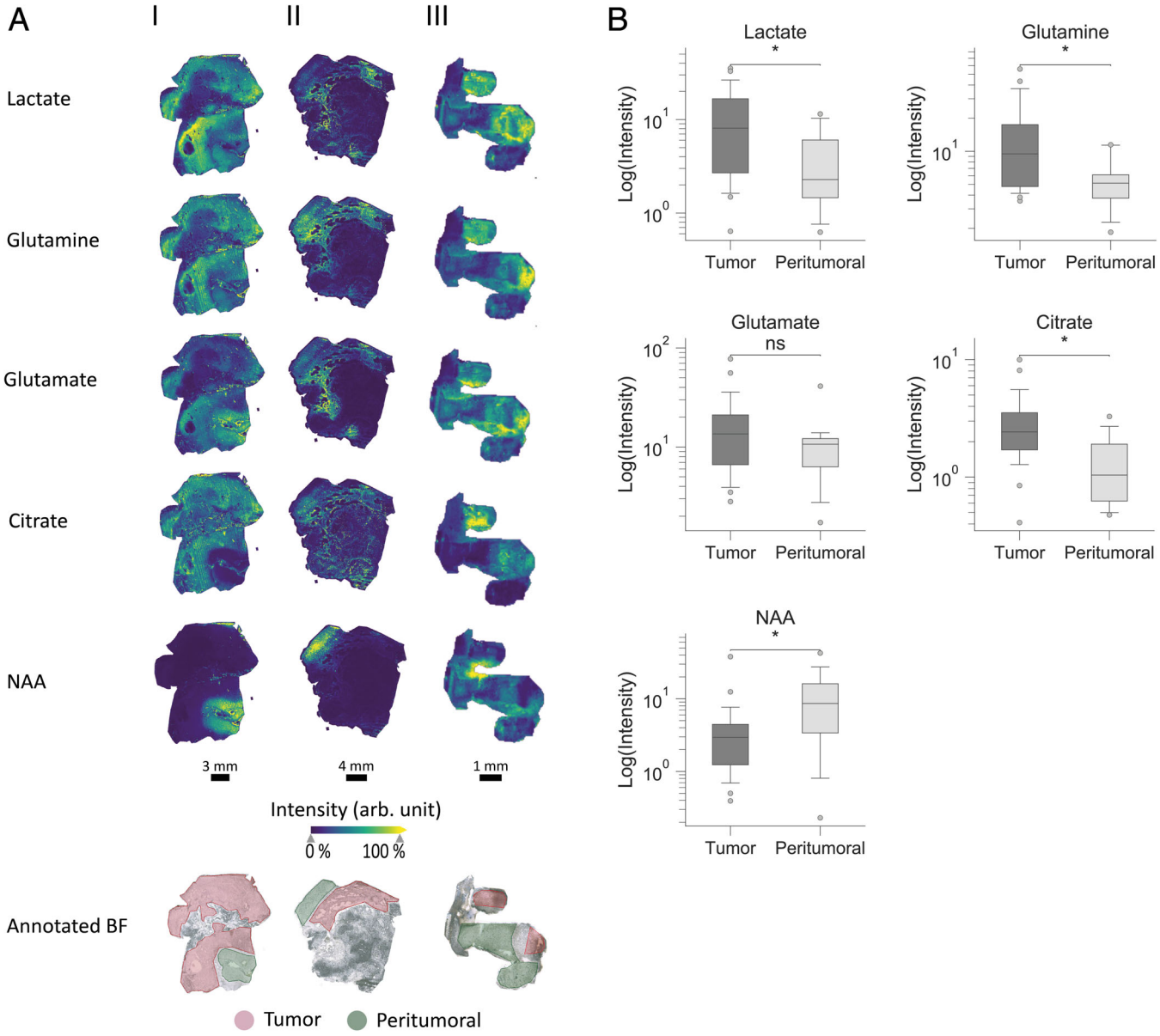

Fig 5 Analyses of further core metabolites in tumor and peritumoral tissue areas of three examples (I–III) by MALDI MSI (A) and intensity boxplots including all 25 GBM samples (B). (A) MALDI-TOF-MSI visualizes lactate, glutamine, glutamate, citrate, and NAA. An annotated brightfield (BF) is included for orientation on tissues. (B) Intensity boxplots for analytes in (A) demonstrate significant alterations. Measurements are performed in negative reflector mode with matrix DAN HCl. Asterisks indicate $P < 0.05$. Tumor group ($n = 25$), Peritumoral group ($n = 13$).

increased intensities in tumor areas with *P*-values of 0.027 and 0.015, respectively, and their levels were highest at areas closed to the tumor areas. Inosine was not altered, while uridine was increased in tumors ($P = 0.024$).

Further metabolites of the core metabolism are altered in GBM

Further metabolites that are involved in tumor metabolism were found to be altered (Fig. 5). Lactate and citrate were significantly increased in tumor areas with *P*-values of 0.023 and 0.015, respectively. Glutamine intensity was also significantly increased in GBM areas ($P = 0.022$), while glutamate showed no consistent alteration for all the samples. In contrast, *N*-acetylaspartate (NAA) was significantly decreased in GBM areas ($P = 0.029$).

Comparison of GBMs with *IDH*-mutated gliomas

Metabolite abundances were compared between *IDH* wild-type GBMs and *IDH*-mutated gliomas (Fig. 6). Antioxidants (taurine, ascorbic acid, and GSH) and

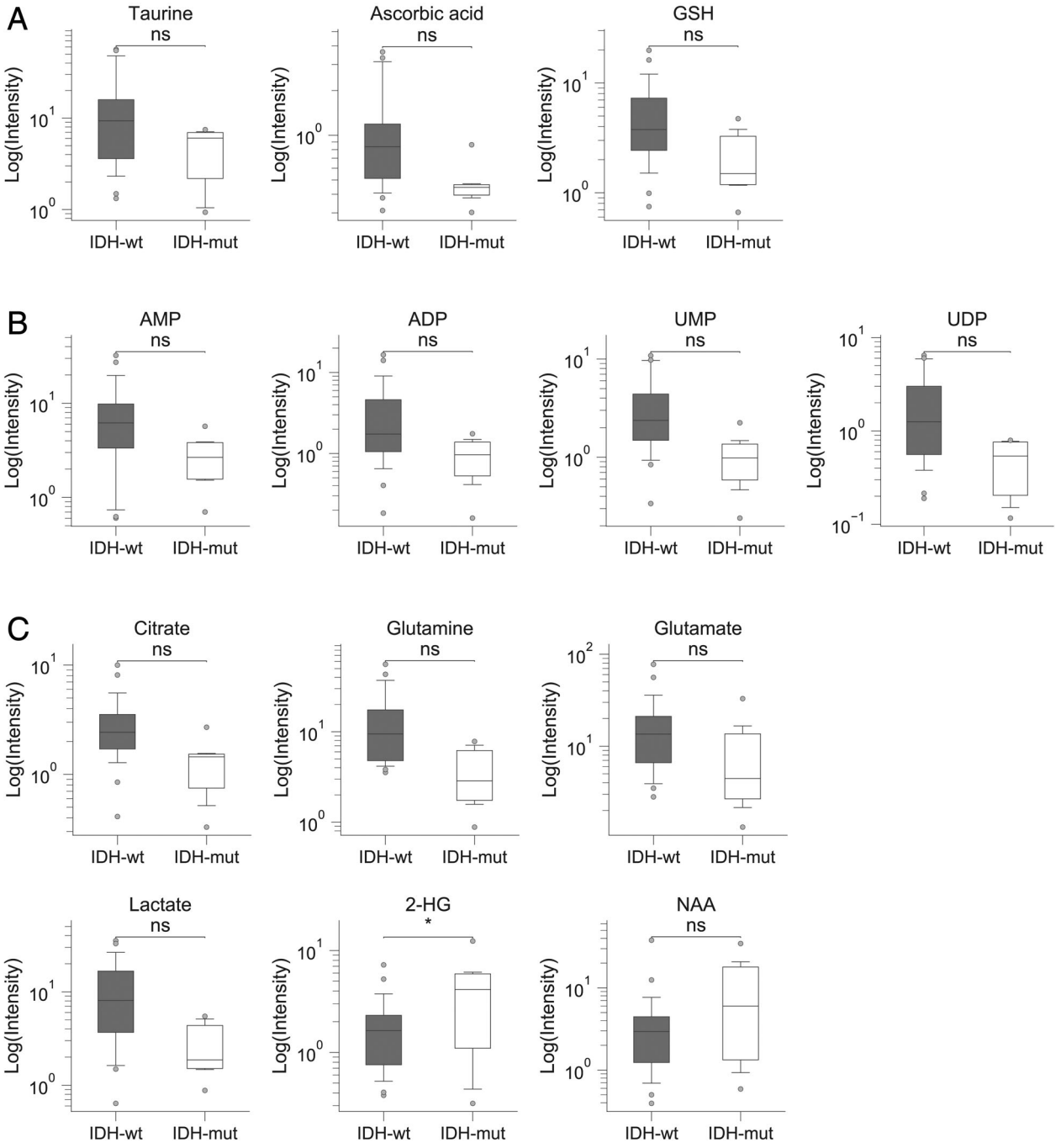

Fig 6 Metabolic differences between *IDH* wild-type GBMs ($n = 25$) and *IDH*-mutated gliomas ($n = 6$). (A) Intensity boxplots tend to show increased levels of antioxidants taurine, ascorbic acid, and GSH in IDH wild-type tumors. (B) Intensity boxplots tend to show increased levels of AMP, ADP, UMP, and UDP. (C) Intensity boxplots tend to show increased levels of typical tumor metabolites citrate, glutamine, glutamate and lactate, while levels of 2-HG and NAA are lower in IDH wild-type tumors. Asterisks indicate $P < 0.05$. ns, not significant.

nucleotides (AMP, ADP, UMP, and UDP) showed higher intensities in *IDH* wild-type GBMs, while not being significantly different. Similar results were observed for metabolites, involved in tumor metabolism (lactate, citrate, glutamine, and glutamate), and an opposite ratio was found for NAA. The oncometabolite 2-HG was significantly increased in *IDH*-mutated gliomas compared to *IDH* wild-type GBM ($P = 0.018$).

DISCUSSION

Antioxidants

Taurine is a β-amino acid which regulates oxidative stress. It enhances the electron transport chain activity in mitochondria and protects them against excessive superoxide generation.[23] In our study, concentrations of taurine were found to be increased in GBM areas. Increased taurine concentrations in gliomas and peritunoral tissue areas compared to extratumoral tissue areas were already detected through high performance liquid chromatography-mass spectrometry (HPLC-MS), and a protective role for the tumor was hypothesized.[24] Extracellular taurine levels were also found to be increased in Grade IV GBM areas and to correlate with cell proliferation.[25] In contrast, reduced taurine levels were detected in a GBM mouse model.[21] The use of glioma models provides a great opportunity in glioma research, although they may not perfectly recapitulate human gliomas.[26]

Another detected strong antioxidant is ascorbic acid, also known as vitamin C. It acts as an important factor for tumor growth and tumor angiogenesis.[27] A high dietary intake of ascorbic acid was associated with decreased survival of glioma patients.[28] Ascorbic acid treatment can protect tumors from radiation damage, the finding observed in a mouse glioma model.[29] Beneficial effects of ascorbic acid treatment for glioma therapy have also been observed.[30,31] To our knowledge, accumulation of ascorbic acid in GBM areas was detected for the first time in this study.

GSH is a highly abundant antioxidant in the human body and was also found to be significantly increased in GBM areas. The same result was obtained in a GBM xenograft.[20] GSH influences initiation and progression in tumorigenesis.[32] It protects cells from free radical damage, and increases the resistance of primary brain tumors against radiotherapy and chemotherapy.[33,34] Moreover, GSH promotes tumor growth under hypoxic conditions.[35]

Fatty acids

Fatty acids are an important source of energy in glioma cells.[36] Abundances of various fatty acids appear decreased in GBM areas. The decreased levels of polyunsaturated fatty acids (PUFA) and cytochrome P-450 as well as the high levels of antioxidants were found to lead to reduced lipid peroxidation in tumor cells.[37] There are different factors that can contribute to the detected reduced concentrations of the ω-6 fatty acid arachidonic acid in GBM areas. The Δ-6-desaturase in part participates in the arachidonic acid synthesis, by desaturating LA to γ-linolenic acid, and shows decreased activity in tumor cells.[38] This can result in less production of arachidonic acid. Enzymes for eicosanoid production are overexpressed in gliomas,[39] hinting at a fast turnover of arachidonic acid. In contrast, increased abundance of arachidonic acid was detected in a mouse model of GBM by MSI.[21] A detection of incorporated fatty acids through in-source decay has to be considered. Nevertheless, an overall alteration of the fatty acid status is detected. As arachidonic acid is the precursor of adrenic acid, detected decreased intensities of adrenic acid in tumor areas are in accordance with these findings. Supplementing the PUFA arachidonic acid induces generation of reactive oxygen species, lipid peroxidation and apoptosis, and limits cell division and tumor growth in glioma cells.[40–42]

The ω-9 fatty acid oleic acid was also found to be significantly decreased in GBM areas. Oleic acid can inhibit cholesterol and fatty acid synthesis in glioma cells.[43,44] Beneficial effects of oleic acid on the promotion of apoptosis in different cancer types have been reported.[45,46] However, the effects of oleic acid in GBM treatment appear to be unexplored.

Purine and pyrimidine metabolites

Extracellular purines and pyrimidines are crucial signaling factors and increase proliferative activity of different glioma cell lines.[47] The purines ATP and adenosine are not detected but are known to have high concentrations in the tumor microenvironment.[48] In the hypoxic tumor, extracellular adenosine accumulates and acts in an immunosuppressive factor.[49] Increased ATP and ADP levels were also detected by MSI in GBM xenografts compared to normal brain.[20] The here observed significantly increased intensities of ADP and AMP in GBM tissue areas are in accordance with the observed decreased ATP and ADP hydrolysis in various glioma cells.[50] A higher hydrolysis rate in the tumor areas close to peritumoral tissue areas can be hypothesized due to the occurring pattern of ADP, being mostly located distantly to peritumoral tissue areas. This tumor heterogeneity is visualized in Figure S5 in Appendix S1.

When analyzing ATP contents, its high conversion rate has to be considered. Methods for rapid quenching in the murine brain include microwave irradiation and freeze-blowing[51,52] but are not applicable to human studies. In this study, collected samples were frozen in liquid nitrogen as soon as possible. Thereby, intensities are assumed to be comparable even if the exact quantity is slightly altered.

The role of pyrimidine metabolites in gliomas is seemingly not as well investigated as the role of purine metabolites. *De novo* pyrimidine synthesis was recently found to be upregulated in GBM stem cells.[53] Furthermore, metabolic analyses of plasma samples from glioma patients revealed increased uridine levels in high-grade gliomas and

GBMs compared to low-grade gliomas and malignant gliomas, respectively.[54] These findings support the here obtained results. UDP, UMP, and uridine abundances are significantly increased in tumor areas, showing a similar heterogeneity for ADP and UDP, as well as for AMP and UMP, respectively.

Lactate

Lactate is produced by tumor cells through anaerobic glycolysis, known as the Warburg effect.[55] Pyruvate is converted to lactate by lactate dehydrogenase (LDH) which is upregulated in various primary tumors, including LDHA upregulated in GBMs.[56,57] In this study, lactate was found to be highly abundant in tumor areas, as already observed by MSI in a human glioma sample by Giampà *et al.* on 2016.[58] Both the inhibition of LDH and the blockage of lactate efflux to glioma microenvironment showed promising results as potential therapeutic targets.[59,56]

Glutamine and glutamate

Cancer cells have a high glutamine uptake dependent on extracellular glutamine levels.[60,61] Glutamine is highly abundant in the brain and is a precursor of different amino acid neurotransmitters, such as glutamate.[62] Glutamine and glutamate levels were found to be increased in GBM areas.[63] In agreement with the published literature, significantly increased glutamine concentrations were detected in GBM areas, where the increase in glutamate was not significant.

Citrate

The tricarboxylic acid (TCA) cycle compound citrate is increased in GBM areas. Citrate was already found to be increased in different studies, including in a GBM mouse model and in aggressive low-grade astrocytomas, suggesting at a glycolysis rate that exceeds the TCA cycle rate.[64,21] Blocking mitochondrial citrate transporter was shown to suppress tumor growth.[65] Moreover, the administration of citrate can also exert anti-tumor effects and can induce apoptosis by inhibiting the glycolysis.[66,67]

NAA

NAA is synthesized in neurons and represents a marker for neuronal health.[68] It can be detected by magnetic resonance spectroscopy and appears to be decreased in tumor areas.[69,70] Consequently, NAA is reduced in human GBM areas, as detected in this study and in previous MALDI MSI studies in xenografts and a GBM mouse model.[21,20] However, NAA treatment of glioma stem-like cells has been observed to enhance cell growth.[71]

IDH-mutated gliomas

It is known that *IDH* mutations lead to the conversion of α-ketoglutarate to 2-HG and the latter accumulation,[72] as also detected in this study. Although other metabolites were not found to be significantly altered, a tendency to peritumoral metabolic status was observed in the lower-graded *IDH* mutant glioma samples compared to *IDH* wild-type GBM samples. Glioma cells overexpressing mutated *IDH* were found to have decreased GSH levels.[73] The here observed minor decrease of GSH levels is in accordance with previous results, where an increased *de novo* biosynthesis of GSH from cysteine was hypothesized.[20] Nevertheless, a consistent slight decrease of antioxidants was detected in *IDH*-mutated gliomas, which is in accordance with the hypothesis that mutant IDH-expressing cells lack cytoprotective activity against oxidative stress[74] and have a higher sensitivity to tumor therapies.[75,76]

Conclusion

In this study, various metabolic alterations in the human GBM were investigated using MALDI MSI and statistical analysis for the first time. This powerful technique enables the label-free visualization of a manifold of analytes on one single tissue section and the differential metabolic evaluation between tumor and peritumoral tissue areas. Antioxidants taurine, ascorbic acid, and GSH are highly abundant in GBM areas compared to peritumoral tissue areas and can thereby protect the tumor against oxidative stress, hypoxia, and therapeutic approaches, and facilitate tumor growth. Purines and pyrimidines were also observed to be increased in tumor areas. Furthermore, different fatty acids were found to be decreased in the tumor areas. While some of them are already investigated well, further research on the effects of fatty acid supplementation may support GBM therapies. Tumor heterogeneity became apparent through metabolite distribution patterns. The detection of tissue levels of NAA, a known marker of neuronal health, along with tumor-associated metabolites including 2-HG and lactate, strengthen the suitability of MSI for the analysis of gliomas to support the decision upon possible therapeutic approaches. In addition, contradictory results in different previous studies hint towards individual variances, as also seen in boxplot visualizations. Metabolic phenotypes of GBMs can be easily investigated for individual patients on one thin section and could possibly contribute to a personalized therapy.

ACKNOWLEDGMENTS

The authors would like to thank Prof. Dr. Carsten Hopf (CH) for the opportunity to perform MALDI MSI

measurements at the Center for Mass Spectrometry and Optical Spectroscopy (CeMOS) at the Mannheim University of Applied Sciences. CH thanks the Deutsche Forschungsgemeinschaft (DFG) for the funding for a SolariX FTICR MS (INST 874/7-1 FUGG) and the Hector-Foundation II for funding for of a RapifleX MS.

DISCLOSURE

The authors declare no conflict of interest.

REFERENCES

1. Ostrom QT, Gittleman H, Truitt G et al. CBTRUS statistical report: Primary brain and other central nervous system tumors diagnosed in the United States in 2011–2015. Neuro Oncol 2018; 20: iv1-iv86.
2. Siebzehnrubl FA, Reynolds BA, Vescovi A, Steindler DA, Deleyrolle LP. The origins of glioma: E pluribus Unum? *Glia* 2011; **59**: 1135–1147.
3. Lim M, Xia Y, Bettegowda C, Weller M. Current state of immunotherapy for glioblastoma. *Nat Rev Clin Oncol* 2018; **15**: 422–442.
4. Stupp R, Mason WP, van den Bent MJ *et al.* European Organisation for Research and Treatment of Cancer Brain Tumor and Radiotherapy Groups, National Cancer Institute of Canada Clinical Trials Group Radiotherapy plus concomitant and adjuvant temozolomide for glioblastoma. *N Engl J Med* 2005; **352**: 987–996.
5. Messaoudi K, Clavreul A, Lagarce F. Toward an effective strategy in glioblastoma treatment. Part I: Resistance mechanisms and strategies to overcome resistance of glioblastoma to temozolomide. *Drug Discovery Today* 2015; **20**: 899–905.
6. Bao S, Wu Q, McLendon RE *et al.* Glioma stem cells promote radioresistance by preferential activation of the DNA damage response. *Nature* 2006; **444**: 756–760.
7. Karsy M, Neil JA, Guan J, Mahan MA, Colman H, Jensen RL. A practical review of prognostic correlations of molecular biomarkers in glioblastoma. *Neurosurg Focus* 2015; **38**: E4.
8. Chen X, Zhang M, Gan H *et al.* A novel enhancer regulates MGMT expression and promotes temozolomide resistance in glioblastoma. *Nat Commun* 2018; **9**: 2949.
9. Weyandt JD, Thompson CB, Giaccia AJ, Rathmell WK. Metabolic alterations in Cancer and their potential as therapeutic targets. *Am Soc Clin Oncol Educ Book* 2017; **37**: 825–832.
10. DeBerardinis RJ, Mancuso A, Daikhin E *et al.* Beyond aerobic glycolysis: Transformed cells can engage in glutamine metabolism that exceeds the requirement for protein and nucleotide synthesis. *Proc Natl Acad Sci U S A* 2007; **104**: 19345–19350.
11. Dong Z, Cui H. Epigenetic modulation of metabolism in glioblastoma. *Semin Cancer Biol* 2019; **57**: 45–51.
12. Quinones A, Le A. The multifaceted metabolism of glioblastoma. In: Le A, (ed). *The Heterogeneity of Cancer Metabolism*. Cham: Springer, 2018; 59–72.
13. Zhou W, Wahl DR. Metabolic abnormalities in Glioblastoma and metabolic strategies to overcome treatment resistance. *Cancers* 2019; **11**: 1231.
14. Pandey R, Caflisch L, Lodi A, Brenner AJ, Tiziani S. Metabolomic signature of brain cancer. *Mol Carcinog* 2017; **56**: 2355–2371.
15. Goodacre R, Vaidyanathan S, Dunn WB *et al.* Metabolomics by numbers: Acquiring and understanding global metabolite data. *Trends Biotechnol* 2004; **22**: 245–252.
16. Niehaus M, Soltwisch J, Belov ME, Dreisewerd K. Transmission-mode MALDI-2 mass spectrometry imaging of cells and tissues at subcellular resolution. *Nat Methods* 2019; **16**: 925–931.
17. Rauser S, Marquardt C, Balluff B *et al.* Classification of HER2 receptor status in breast cancer tissues by MALDI imaging mass spectrometry. *J Proteome Res* 2010; **9**: 1854–1863.
18. Schwamborn K, Krieg RC, Reska M *et al.* Identifying prostate carcinoma by MALDI-Imaging. *Int J Mol Med* 2007; **20**: 155–159.
19. El Ayed M, Bonnel D, Longuespée R *et al.* MALDI imaging mass spectrometry in ovarian cancer for tracking, identifying, and validating biomarkers. *Med Sci Monit* 2010; **16**: BR233–BR245.
20. Fack F, Tardito S, Hochart G *et al.* Altered metabolic landscape in IDH-mutant gliomas affects phospholipid, energy, and oxidative stress pathways. *EMBO Mol Med* 2017; **9**: 1681–1695.
21. Dilillo M, Ait-Belkacem R, Esteve C *et al.* Ultra-high mass resolution MALDI imaging mass spectrometry of proteins and metabolites in a mouse model of Glioblastoma. *Sci Rep* 2017; **7**: 603.
22. Liu H, Chen R, Wang J *et al.* 1,5-Diaminonaphthalene hydrochloride assisted laser desorption/ionization mass spectrometry imaging of small molecules in tissues following focal cerebral ischemia. *Anal Chem* 2014; **86**: 10114–10121.
23. Jong CJ, Azuma J, Schaffer S. Mechanism underlying the antioxidant activity of taurine: Prevention of mitochondrial oxidant production. *Amino Acids* 2012; **42**: 2223–2232.
24. Cubillos S, Obregón F, Vargas MF *et al.* Taurine concentration in human gliomas and meningiomas: Tumoral, peritumoral, and extratumoral tissue. *Adv Exp Med Biol* 2006; **583**: 419–422.

25. Bianchi L, De Micheli E, Bricolo A *et al*. Extracellular levels of amino acids and choline in human high grade Gliomas: An intraoperative microdialysis study. *Neurochem Res* 2004; **29**: 325–334.
26. Lenting K, Verhaak R, Ter Laan M *et al*. Glioma: Experimental models and reality. *Acta Neuropathol* 2017; **133**: 263–282.
27. Telang S, Clem AL, Eaton JW, Chesney J. Depletion of ascorbic acid restricts angiogenesis and retards tumor growth in a mouse model. *Neoplasia* 2007; **9**: 47–56.
28. DeLorenze GN, McCoy L, Tsai A-L *et al*. Daily intake of antioxidants in relation to survival among adult patients diagnosed with malignant glioma. *BMC Cancer* 2010; **10**: 215.
29. Grasso C, Fabre M-S, Collis SV *et al*. Pharmacological doses of daily ascorbate protect tumors from radiation damage after a single dose of radiation in an intracranial mouse glioma model. *Front Oncol* 2014; **4**: 356.
30. Baillie N, Carr AC, Peng S. The use of intravenous vitamin C as a supportive therapy for a patient with Glioblastoma Multiforme. *Antioxidants* 2018; **7**: 115.
31. Schoenfeld JD, Sibenaller ZA, Mapuskar KA et al. O2·- and H2O2-mediated disruption of Fe metabolism causes the differential susceptibility of NSCLC and GBM cancer cells to pharmacological ascorbate. Cancer Cell 2017; 31: 487-500.e8.
32. Bansal A, Simon MC. Glutathione metabolism in cancer progression and treatment resistance. *J Cell Biol* 2018; **217**: 2291–2298.
33. Backos DS, Franklin CC, Reigan P. The role of glutathione in brain tumor drug resistance. *Biochem Pharmacol* 2012; **83**: 1005–1012.
34. Bump EA, Brown JM. Role of glutathione in the radiation response of mammalian cells in vitro and in vivo. *Pharmacol Ther* 1990; **47**: 117–136.
35. Ogunrinu TA, Sontheimer H. Hypoxia increases the dependence of glioma cells on glutathione. *J Biol Chem* 2010; **285**: 37716–37724.
36. Strickland M, Stoll EA. Metabolic reprogramming in Glioma. *Front Cell Dev Biol* 2017; **5**: 43.
37. Cheeseman KH, Burton GW, Ingold KU, Slater TF. Lipid peroxidation and lipid antioxidants in Normal and tumor cells. *Toxicol Pathol* 1984; **12**: 235–239.
38. Das UN. From bench to the clinic: Γ-linolenic acid therapy of human gliomas. *Prostaglandins Leukot Essent Fatty Acids* 2004; **70**: 539–552.
39. Nathoo N. The eicosanoid cascade: Possible role in gliomas and meningiomas. *J Clin Pathol* 2004; **57**: 6–13.
40. Leaver HA, Williams JR, Smith C, Whittle IR. Intracellular oxidation by human glioma cell populations: Effect of arachidonic acid. *Prostaglandins Leukot Essent Fatty Acids* 2004; **70**: 449–453.
41. Williams JR, Leaver HA, Ironside JW, Miller EP, Whittle IR, Gregor A. Apoptosis in human primary brain tumours: Actions of arachidonic acid. *Prostaglandins Leukot Essent Fatty Acids* 1998; **58**: 193–200.
42. Liepkalns VA, Icard-Liepkalns C, Cornwell DG. Regulation of cell division in a human glioma cell clone by arachidonic acid and α-tocopherolquinone. *Cancer Lett* 1982; **15**: 173–178.
43. Priore P, Gnoni A, Natali F *et al*. Oleic acid and Hydroxytyrosol inhibit cholesterol and fatty acid synthesis in C6 Glioma cells. *Oxid Med Cell Longev* 2017; **2017**: 1–10.
44. Natali F, Siculella L, Salvati S, Gnoni GV. Oleic acid is a potent inhibitor of fatty acid and cholesterol synthesis in C6 glioma cells. *J Lipid Res* 2007; **48**: 1966–1975.
45. Menendez JA, Vellon L, Colomer R *et al*. Oleic acid, the main monounsaturated fatty acid of olive oil, suppresses Her-2/neu (erbB-2) expression and synergistically enhances the growth inhibitory effects of trastuzumab (Herceptin™) in breast cancer cells with Her-2/neu oncogene amplification. *Ann Oncol* 2005; **16**: 359–371.
46. Jiang L, Wang W, He Q *et al*. Oleic acid induces apoptosis and autophagy in the treatment of tongue squamous cell carcinomas. *Sci Rep* 2017; **7**: 1–11.
47. Morrone FB, Jacques-Silva MC, Horn AP *et al*. Extracellular nucleotides and nucleosides induce proliferation and increase nucleoside transport in human Glioma cell lines. *J Neurooncol* 2003; **64**: 211–218.
48. Di Virgilio F, Adinolfi E. Extracellular purines, purinergic receptors and tumor growth. *Oncogene* 2017; **36**: 293–303.
49. Ohta A. A metabolic immune checkpoint: Adenosine in tumor microenvironment. *Front Immunol* 2016; **7**: 109.
50. Wink MR, Lenz G, Braganhol E *et al*. Altered extracellular ATP, ADP and AMP catabolism in glioma cell lines. *Cancer Lett* 2003; **198**: 211–218.
51. Medina MA, Jones DJ, Stavinoha WB, Ross DH. The levels of labile intermediary metabolites in mouse brain following rapid tissue fixation with microwave irradiation. *J Neurochem* 1975; **24**: 223–227.
52. Veech RL, Harris RL, Veloso D, Veech EH. Freeze-blowing: A new technique for the study of brain in vivo. *J Neurochem* 1973; **20**: 183–188.
53. Wang X, Yang K, Wu Q et al. Targeting pyrimidine synthesis accentuates molecular therapy response in glioblastoma stem cells. Sci Transl Med 2019; 11, eaau4972.

54. Zhao H, Heimberger AB, Lu Z *et al*. Metabolomics profiling in plasma samples from glioma patients correlates with tumor phenotypes. *Oncotarget* 2016; **7**: 20486–20495.
55. Warburg O, Wind F, Negelein E. The metabolism of tumors in the body. *J Gen Physiol* 1927; **8**: 519–530.
56. Li J, Zhu S, Tong J *et al*. Suppression of lactate dehydrogenase a compromises tumor progression by down-regulation of the Warburg effect in glioblastoma. *Neuroreport* 2016; **27**: 110–115.
57. Walenta S, Mueller-Klieser WF. Lactate: Mirror and motor of tumor malignancy. *Semin Radiat Oncol* 2004; **14**: 267–274.
58. Giampà M, Lissel MB, Patschkowski T *et al*. Maleic anhydride proton sponge as a novel MALDI matrix for the visualization of small molecules (<250 m/z) in brain tumors by routine MALDI ToF imaging mass spectrometry. *Chem Commun* 2016; **52**: 9801–9804.
59. Colen CB, Shen Y, Ghoddoussi F *et al*. Metabolic targeting of lactate efflux by malignant Glioma inhibits invasiveness and induces necrosis: An in vivo Study1. *Neoplasia* 2011; **13**: 620–632.
60. Altman BJ, Stine ZE, Dang CV. From Krebs to clinic: Glutamine metabolism to cancer therapy. *Nat Rev Cancer* 2016; **16**: 619–634.
61. Wise DR, Thompson CB. Glutamine addiction: A new therapeutic target in Cancer. *Trends Biochem Sci* 2010; **35**: 427–433.
62. Albrecht J, Sidoryk-Węgrzynowicz M, Zielińska M, Aschner M. Roles of glutamine in neurotransmission. *Neuron Glia Biol* 2010; **6**: 263–276.
63. Tanaka K, Sasayama T, Irino Y *et al*. Compensatory glutamine metabolism promotes glioblastoma resistance to mTOR inhibitor treatment. *J Clin Invest* 2015; **125**: 1591–1602.
64. Blüml S, Panigrahy A, Laskov M *et al*. Elevated citrate in pediatric astrocytomas with malignant progression. *Neuro Oncol* 2011; **13**: 1107–1117.
65. Mycielska ME, Dettmer K, Rummele P *et al*. Extracellular citrate affects critical elements of Cancer cell metabolism and supports Cancer development in vivo. *Cancer Res* 2018; **78**: 2513–2523.
66. Icard P, Poulain L, Lincet H. Understanding the central role of citrate in the metabolism of cancer cells. *Biochim Biophys Acta* 1825; **2012**: 111–116.
67. Sayed SME, Baghdadi HH, Omar NAA *et al*. The antioxidant glycolysis inhibitor (citric acid) induces a dose-dependent caspase-mediated apoptosis and necrosis in glioma cells. *J Cancer Res Treat* 2018; **6**: 18–24.
68. Moffett JR, Ross B, Arun P *et al*. N-Acetylaspartate in the CNS: From neurodiagnostics to neurobiology. *Prog Neurobiol* 2007; **81**: 89–131.
69. Bruhn H, Frahm J, Gyngell ML *et al*. Noninvasive differentiation of tumors with use of localized H-1 MR spectroscopy in vivo: Initial experience in patients with cerebral tumors. *Radiology* 1989; **172**: 541–548.
70. Verma A, Kumar I, Verma N, Aggarwal P, Ojha R. Magnetic resonance spectroscopy - revisiting the biochemical and molecular milieu of brain tumors. *BBA Clin* 2016; **5**: 170–178.
71. Long PM, Moffett JR, Namboodiri AMA *et al*. N-Acetylaspartate (NAA) and N-Acetylaspartylglutamate (NAAG) promote growth and inhibit differentiation of glioma stem-like cells. *J Biol Chem* 2013; **288**: 26188–26200.
72. Dang L, White DW, Gross S *et al*. Cancer-associated IDH1 mutations produce 2-hydroxyglutarate. *Nature* 2009; **462**: 739–744.
73. Shi J, Zuo H, Ni L *et al*. An IDH1 mutation inhibits growth of glioma cells via GSH depletion and ROS generation. *Neurol Sci* 2014; **35**: 839–845.
74. Mohrenz IV, Antonietti P, Pusch S *et al*. Isocitrate dehydrogenase 1 mutant R132H sensitizes glioma cells to BCNU-induced oxidative stress and cell death. *Apoptosis* 2013; **18**: 1416–1425.
75. Tran AN, Lai A, Li S *et al*. Increased sensitivity to radiochemotherapy in IDH1 mutant glioblastoma as demonstrated by serial quantitative MR volumetry. *Neuro Oncol* 2014; **16**: 414–420.
76. Khurshed M, Aarnoudse N, Hulsbos R *et al*. IDH1-mutant cancer cells are sensitive to cisplatin and an IDH1-mutant inhibitor counteracts this sensitivity. *FASEB J* 2018; **32**(11): 6344–6352.

SUPPORTING INFORMATION

Additional supporting information may be found in the online version of this article at the publisher's website: http://onlinelibrary.wiley.com/doi//suppinfo.

Appendix S1. Supporting Information.